CFD Letters www.cfdl.issres.net Vol. 2 (1) – March 2010

Simulation of Incompressible Flows in Two-Sided Lid-Driven Square Cavities. Part I - FDM

D. Arumuga Perumal[1c] and Anoop K. Dass[1]
[1] *Department of Mechanical Engineering,*
Indian Institute of Technology Guwahati,
Guwahati-781039, INDIA

Received: 15/10/2009 – Revised 08/01/2010 – Accepted 01/03/2010

Abstract

The present paper computes the flow in a two-sided lid-driven square cavity by finite difference method (FDM). The two-sided lid-driven cavity problem has multiple steady solutions for some aspect ratios. However, for the square cavity, the problem gives only a single steady solution for both the parallel and antiparallel motion of the walls. Unlike one-sided lid-driven cavity flows involving wall shear layer and their separation, the two-sided cavity flow with parallel wall motion also involve a free shear layer and different vortex patterns. The problem therefore merits careful investigation, which is attempted in this paper through the finite difference method for various Reynolds numbers for both the parallel and antiparallel motion of the walls.

Keywords: two-sided lid-driven square cavity; finite difference method; parallel wall motion; antiparallel wall motion; alternate direction implicit method.

1. Introduction

Numerical simulation of fluid flow has been a major topic of research for the past few decades [1]. Computational fluid dynamics (CFD) involves describing the fluid flow in terms of mathematical models that include convective and diffusive transport of some variables. These mathematical models consist of governing equations in the form of ordinary or partial differential equations. As a great number of such model equations like the Navier-Stokes equations do not possess analytical solutions, one has to resort to numerical methods. In conventional numerical methods the macroscopic variables of interest, such as velocity and pressure are usually obtained by solving the Navier-Stokes equations. Over the years, finite difference method is frequently used in CFD. FDM consists in essentially setting up a uniform grid in the problem domain, discretizing the governing equations with respect to the grid by replacing the derivatives with their finite-difference approximations and solving the resulting algebraic equations numerically. It is known that, the lid-driven cavity flow problem is not only technically important but also of great scientific interest because it displays almost all fluid mechanical phenomena in the simplest geometrical settings [2]. This problem is also attractive because of its importance in industrial applications such as coating &

[c] Corresponding Author: D. Arumuga Perumal
Email: d.perumal@iitg.ernet.in Telephone: +91 361 2582654 Fax: +91 361 2690762

drying technologies, melt spinning processes and many others [3]. A number of experimental and numerical studies have been conducted to investigate the flow field of a lid-driven cavity flow in the last several decades [4-7]. Ghia et al. [7] have applied a multi-grid strategy and presented solutions for Reynolds numbers starting from Re = 100 to as high as Re = 10000. Kuhlmann and other investigators [8-10] have done several experiments on two-sided lid-driven cavity with various spanwise aspect ratios. Blohm and Kuhlmann [9] experimentally investigated the incompressible fluid flow in a rectangular container driven by two facing sidewalls which move steadily in an anti-parallel direction up to Re = 1200. Albensoeder et al. [10] were among the first to investigate the nonlinear regime and found multiple two-dimensional states in rectangular cavities. They have found seven and five flow states in antiparallel and parallel motion respectively. Kalita et al. [11] developed an HOC algorithm for Stream-function vorticity formulation of the 2D N-S equations on graded Cartesian meshes. Kumar et al. [12] used the algorithm to compute the flow in a two-sided 2D lid-driven cavity where, besides wall shear, free shear flow is also encountered. The present work is concerned with the computation of two-sided lid-driven square cavity flows by Finite Difference Method. The alternate direction implicit (ADI) method [13] is used for time integration.

This paper is organized in four sections. In Section 2, stream function-vorticity based FDM is described in some detail. In Section 3, the two-sided lid-driven cavity problem is described and the results with parallel and antiparallel motion of the walls are presented. Concluding remarks are made in Section 4.

2. Numerical Method

2.1. Stream Function-Vorticity Based Finite Difference Solver

The Finite Difference code numerically solves the 2D Navier-Stokes equations in the stream function-vorticity form given by

$$\frac{\partial^2 \psi}{\partial x^2} + \frac{\partial^2 \psi}{\partial y^2} = -\omega \tag{1}$$

$$\frac{\partial \omega}{\partial \mathrm{t}} + u\frac{\partial \omega}{\partial x} + v\frac{\partial \omega}{\partial y} = \frac{1}{Re}\left(\frac{\partial^2 \omega}{\partial x^2} + \frac{\partial^2 \omega}{\partial y^2}\right). \tag{2}$$

It is intended to obtain the steady state solution from the discretized equations in a time marching fashion. It is well known that in an explicit technique that uses a forward time-stepping of first order accuracy and a central spatial discretization, the stability limit restricts the time-step to a very small value and the convergence to the steady state is painfully slow. This is especially true for larger Reynolds numbers at which it is extremely difficult to obtain the steady state solution when central space-differencing is used. To overcome this problem a first order accurate one sided space-differencing can be used in the convective term. This however, limits accuracy of the results and is no solution to the problem encountered. Maintaining a good spatial accuracy of second order by using central space-differencing and adopting an implicit time stepping through alternate direction implicit (ADI) technique that improves the stability behaviour of the computation remarkably, we circumvent this problem and obtain accurate solutions at higher Reynolds numbers as well. Since we intend to use the present code to complete the flow in a two-sided square cavity, for which no earlier results exist, the code requires to be validated first.

2.2. Validation of Finite Difference-Based ADI Code

As a precursor to the problem of two-sided lid-driven cavity, the performance and accuracy of the present computational strategy is first ascertained through the single lid-driven cavity problem by way of code validation. Consequently, the developed FDM code is used to compute the single lid-driven square cavity flow for Re = 1000 on a 129 × 129

grid. Well-established results computed by Ghia et al. [7] exist for the same problem on a similar grid, which are used for the present code-validation exercise. Figures 1(a) and 1(b) shows the steady-state *x*-component of the velocity along the vertical centreline and the *y*-component of the velocity along the horizontal centreline of the cavity at *Re* = 1000. Here the top lid moves from left to right and it is observed that the agreement between our results and those of Ghia et al. [7] is excellent. The close agreement gives credibility to the result of our FDM code and it stands validated. In the next section the FDM results for the unexplored two-sided lid-driven cavity flow will be presented.

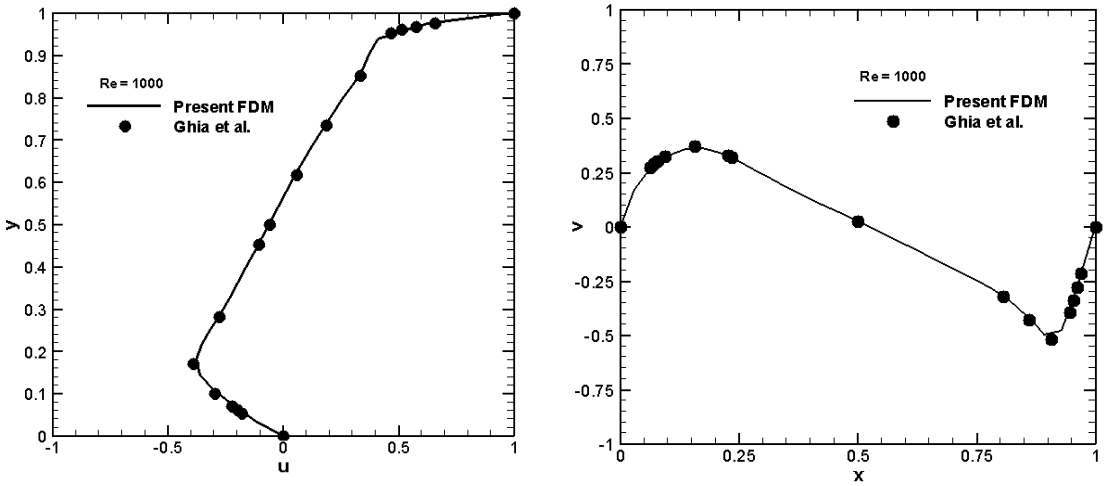

Figure 1. Code validation: (a) *u*-velocity along vertical centreline and (b) *v*-velocity along horizontal centreline for single lid-driven square-cavity (*Re* = 1000).

3. Two-Sided Lid-Driven Square Cavity Flow

An incompressible viscous flow in a square cavity whose top and bottom walls move in the same (parallel motion) or opposite (antiparallel motion) direction with a uniform velocity is the problem investigated in the present work. In the case of parallel wall motion, a free shear layer exists midway between the top and bottom walls apart from the wall bounded shear layers, whereas in the case of antiparallel wall motion, only wall bounded shear layers exist. The boundary conditions for parallel and antiparallel wall motion cases are shown in the Figure 2 (a) and 2 (b).

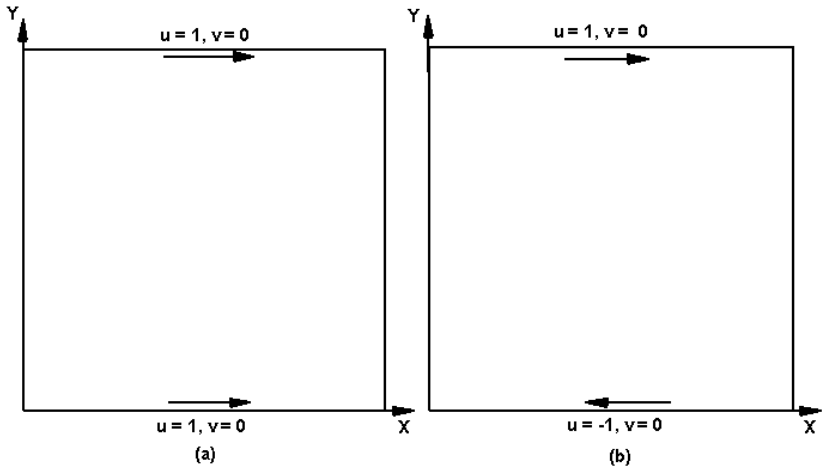

Figure 2. Two-Sided Lid-Driven Cavity for (a) parallel wall motion (b) antiparallel wall motion with moving wall boundary conditions.

3.1. Parallel Wall Motion

Figure 3 shows the streamline patterns obtained using a 257 × 257 grid for *Re* = 100, 400, 1000 and 2000. Here the upper and lower walls move in the same direction along the *x*-axis with the same velocity. The streamlines are found to be symmetrical with respect to a line parallel to these walls and passing through the cavity centre.

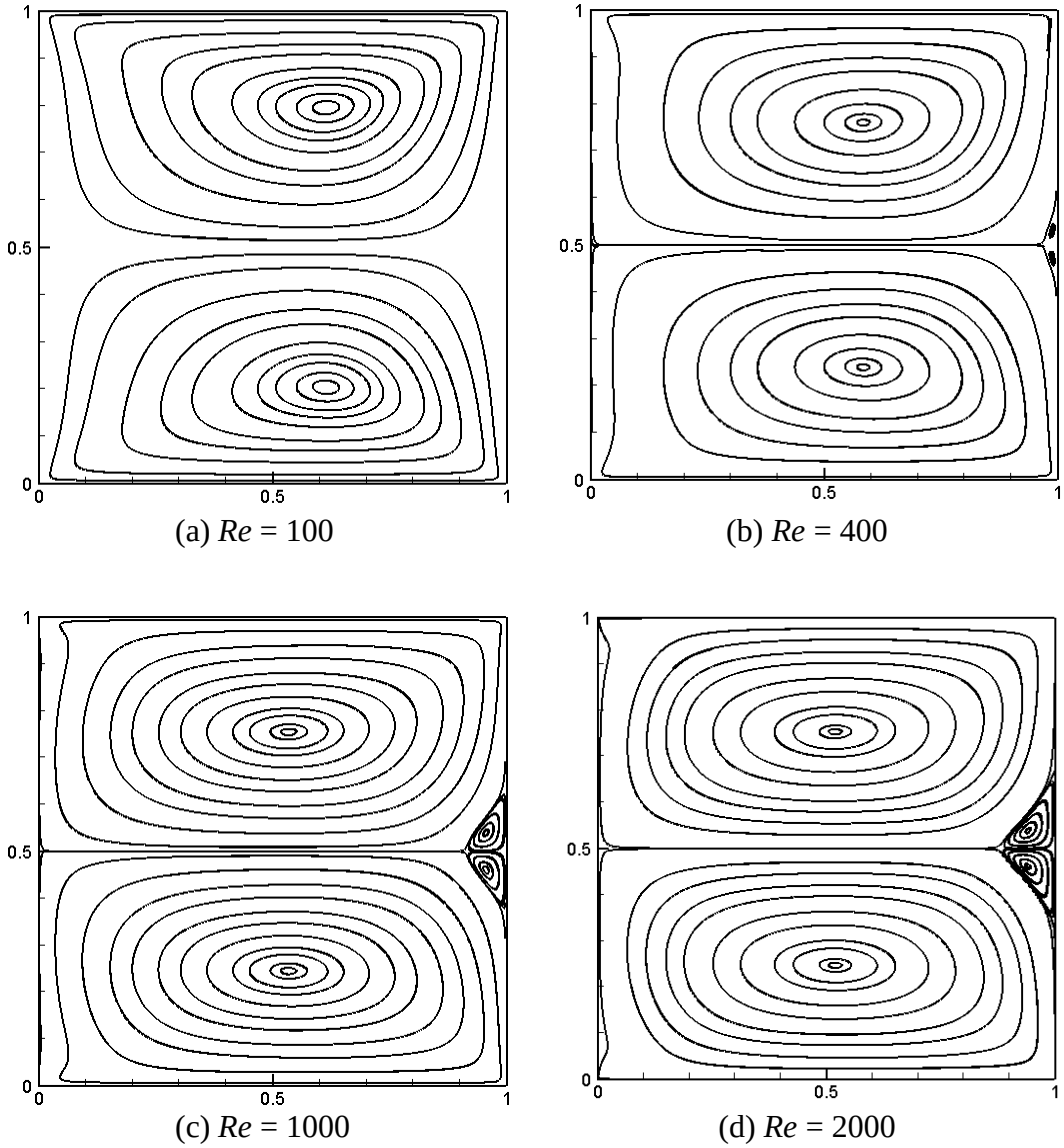

(a) *Re* = 100 (b) *Re* = 400

(c) *Re* = 1000 (d) *Re* = 2000

Figure 3. Streamline pattern for parallel wall motion at (a) *Re* = 100 (b) *Re* = 400 (c) *Re* = 1000 and (d) *Re* = 2000 on a 257 × 257 grid.

Figure 3(a) shows the streamline pattern for the parallel wall motion at *Re* = 100 with the top and bottom walls moving from the left to right. Two counter-rotating primary vortices symmetrical to each other are seen to form with a free shear layer in between. At this Reynolds number the primary vortex cores are seen to be somewhat away from the centres of the top and the bottom halves of the cavity towards the righthand top and righthand bottom corners respectively. At *Re* = 400 (Figure 3(b)), apart from the primary vortices a pair of counter-rotating secondary vortices symmetrically placed about the horizontal centreline are seen to appear near the centre of the right wall. Figures 3(c) and 3(d) show the streamline patterns at *Re* = 1000 and *Re* = 2000 respectively. From Figure 3 it

is observed that as the Reynolds number increases the cores of the primary vortices move from near the top right and bottom right corners towards the centres of the top and bottom halves of the cavity respectively. As the Reynolds number increases the secondary vortices near the centre of the right wall grow in size. The counter-rotating pairs of primary and secondary vortices maintain their symmetry at all the Reynolds numbers investigated here. Figure 4 shows the vorticity contours for the various Reynolds numbers. A magnified view of the secondary vortices at *Re* = 1000 obtained for the parallel wall motion is shown in Figure 5.

Figures 6-9 show plots of horizontal velocity profiles along vertical lines and vertical velocity profiles along horizontal lines passing through different points of the square cavity for various Reynolds numbers. Table 1 gives the locations of the vortex centres for *Re* = 100, 400, 1000, 1500 and 2000. Considering the fact that the present code has second-order spatio-temporal accuracy and it has been adequately validated, the listings of various flow details for this untested configuration should be accurate.

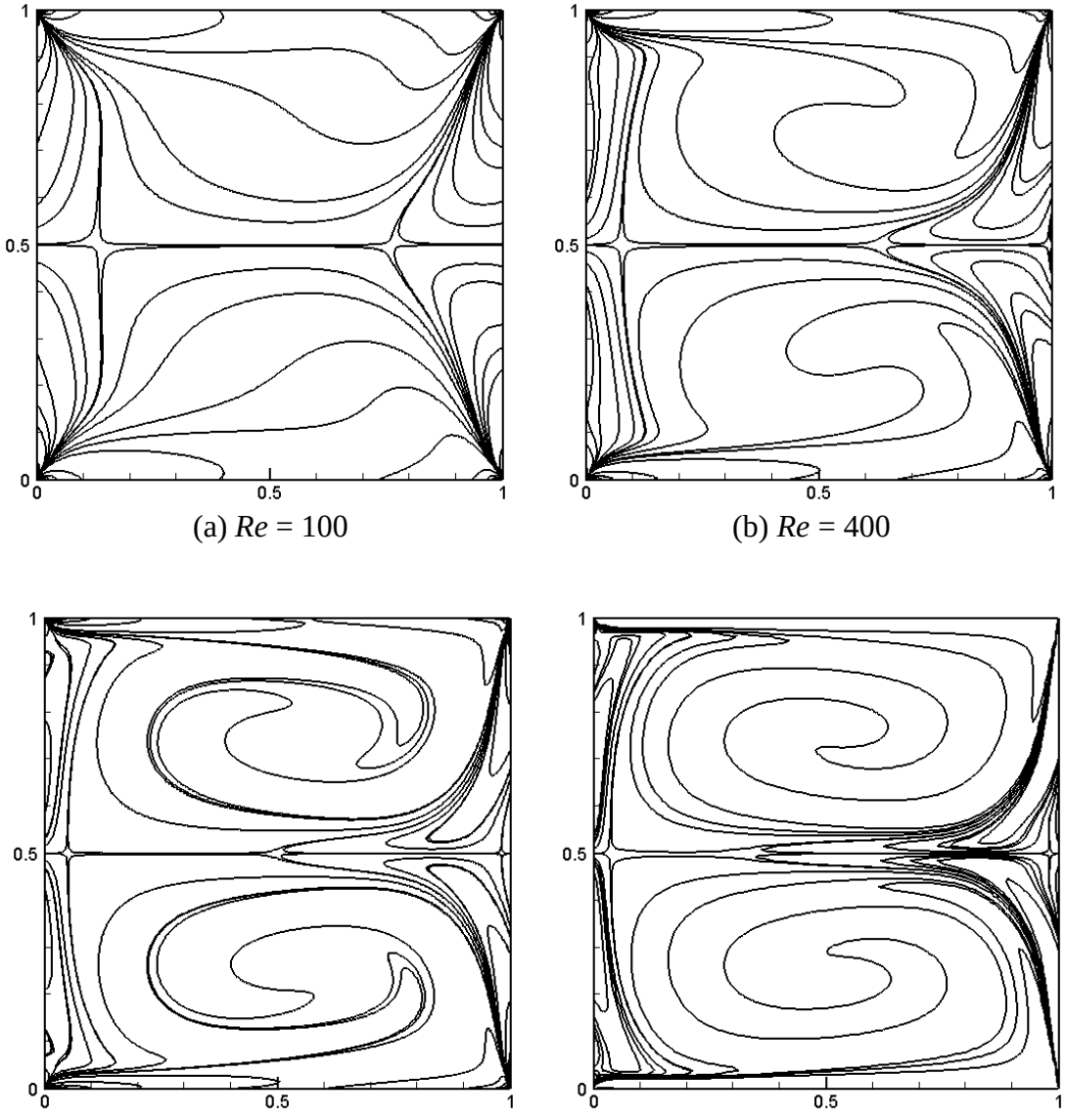

(a) *Re* = 100 (b) *Re* = 400

(c) *Re* = 1000 (d) *Re* = 2000

Figure 4. Vorticity contours for parallel wall motion at (a) *Re* = 100 (b) *Re* = 400 (c) *Re* = 1000 and (d) *Re* = 2000 on a 257 × 257 grid.

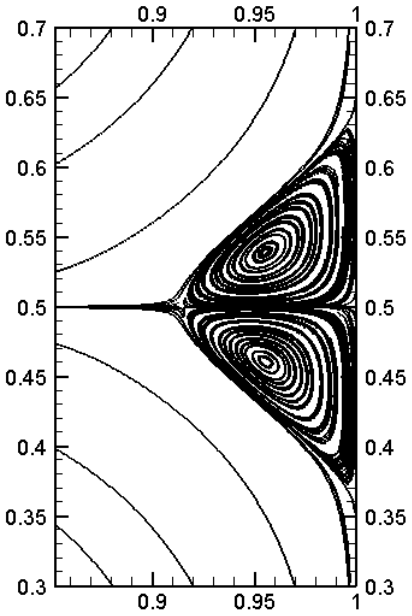

Figure 5. A magnified view of secondary vortices for parallel wall motion (*Re* = 1000).

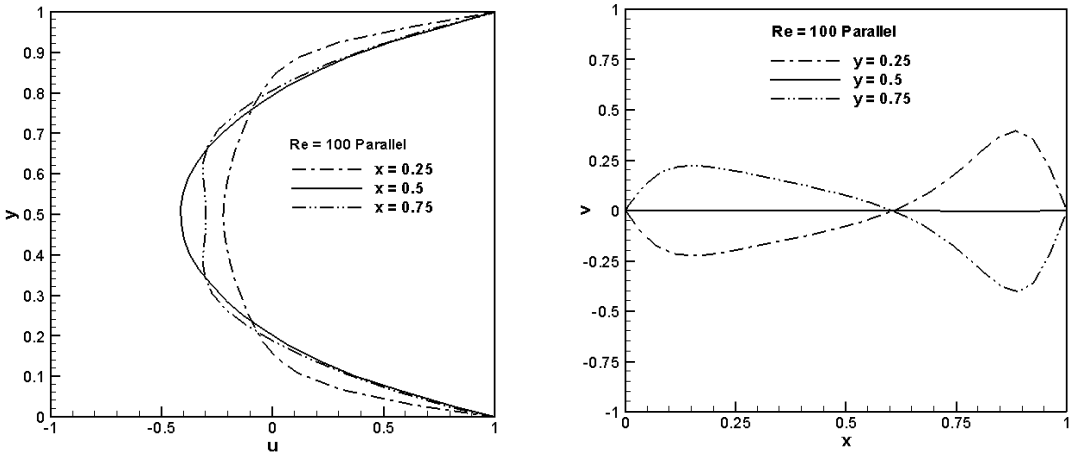

Figure 6. Parallel wall motion, *Re* = 100: (a) horizontal velocity *u* along vertical lines (*x*=0.25, 0.50, 0.75), (b) vertical velocity *v* along horizontal lines (*y*=0.25, 0.50, 0.75).

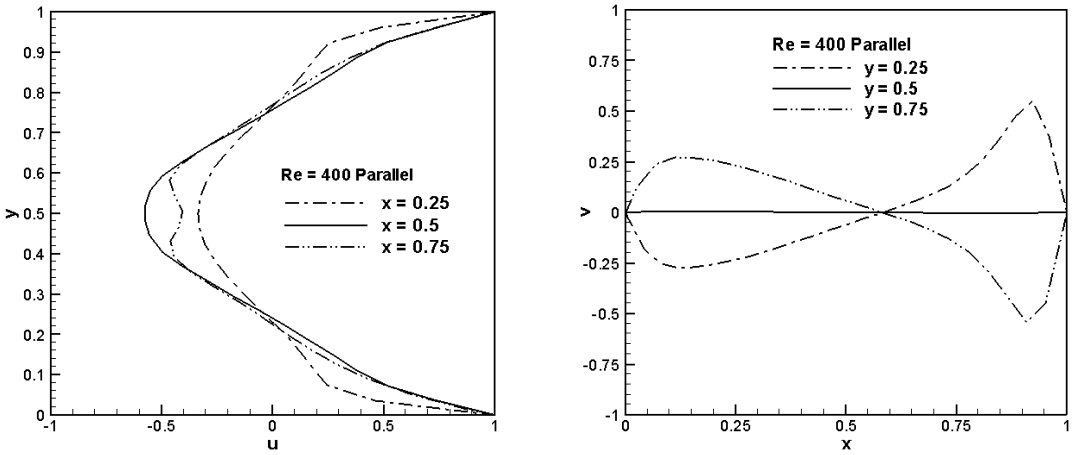

Figure 7. Parallel wall motion, *Re* = 400: (a) horizontal velocity *u* along vertical lines (*x*=0.25, 0.50, 0.75), (b) vertical velocity *v* along horizontal lines (*y*=0.25, 0.50, 0.75).

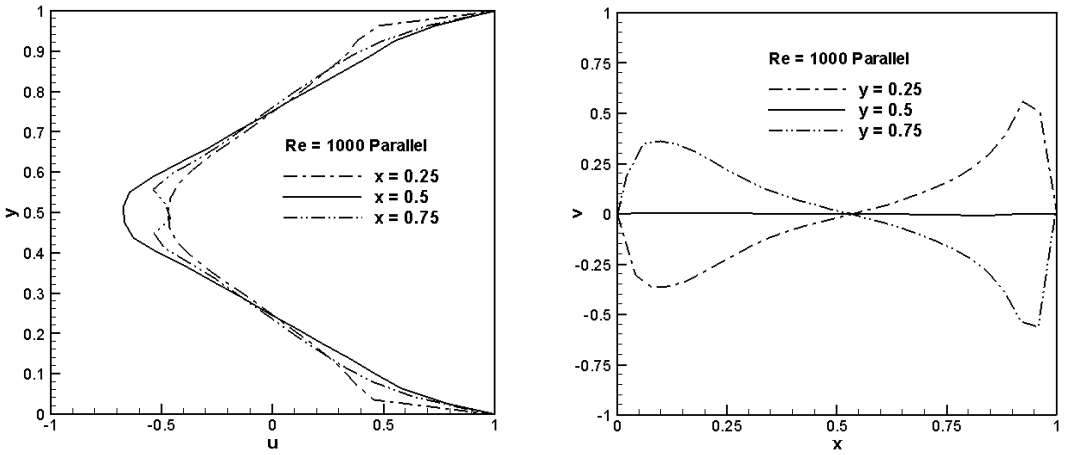

Figure 8. Parallel wall motion, *Re* = 1000: (a) horizontal velocity *u* along vertical lines (*x*=0.25, 0.50, 0.75), (b) vertical velocity *v* along horizontal lines (*y*=0.25, 0.50, 0.75).

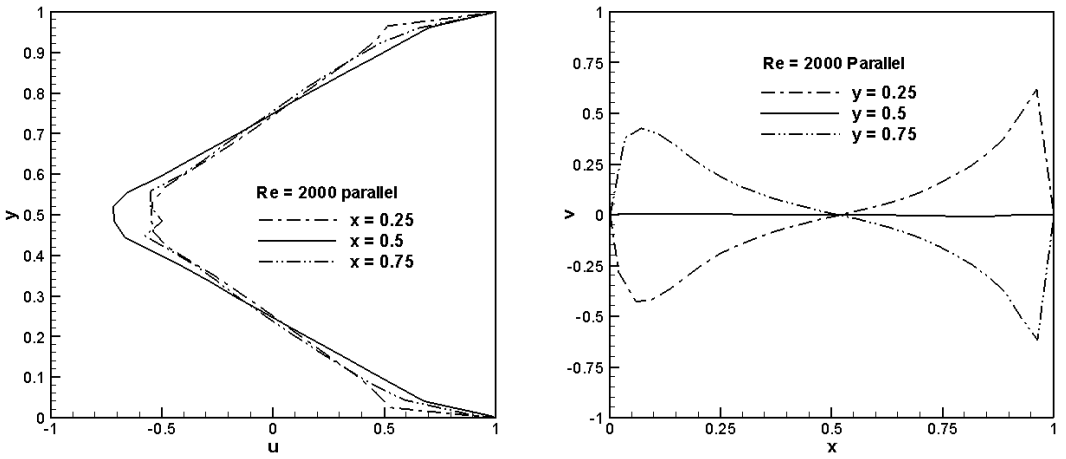

Figure 9. Parallel wall motion, *Re* = 2000: (a) horizontal velocity *u* along vertical lines (*x*=0.25, 0.50, 0.75), (b) vertical velocity *v* along horizontal lines (*y*=0.25, 0.50, 0.75).

TABLE 1: LOCATIONS OF THE VORTICES FOR PARALLEL WALL MOTION USING FDM.

Re	Primary vortex centres				Secondary vortex centres			
	Bottom		Top		Bottom		Top	
	x	*y*	*x*	*y*	*x*	*y*	*x*	*y*
100	0.6145	0.2026	0.6145	0.7959	…	…	…	…
400	0.5845	0.2388	0.5845	0.7553	0.9873	0.4638	0.9873	0.5264
1000	0.5354	0.2452	0.5354	0.7547	0.9551	0.4570	0.9551	0.5409
1500	0.5246	0.2452	0.5251	0.7527	0.9443	0.4569	0.9444	0.5429
2000	0.5132	0.2474	0.5132	0.7528	0.9400	0.4573	0.9400	0.5478

3.2. Antiparallel Wall Motion

Figure 10 gives the streamline patterns obtained on a 257 × 257 grid for *Re* = 100, 400, 1000 and 2000. Here the upper and lower walls move in opposite directions along the *x*-axis with the same velocity. A single primary vortex centered at the geometric centre of the cavity is formed at low Reynolds numbers (Figures 10(a) and 10(b)). These two figures show the streamline patterns for *Re* = 100 and 400 respectively. Figures 10(c) and 10(d) depict the streamline patterns for *Re* = 1000 and 2000 showing the appearance of two secondary vortices near the top left and the bottom right corners of the cavity and a very small shift of the primary vortex centre from the geometric centre of the cavity. It may be noted that the corresponding secondary vortex for a single lid-driven cavity flow does not appear at a Reynolds number as low as 1000 but much beyond that (at some value higher than 2000).

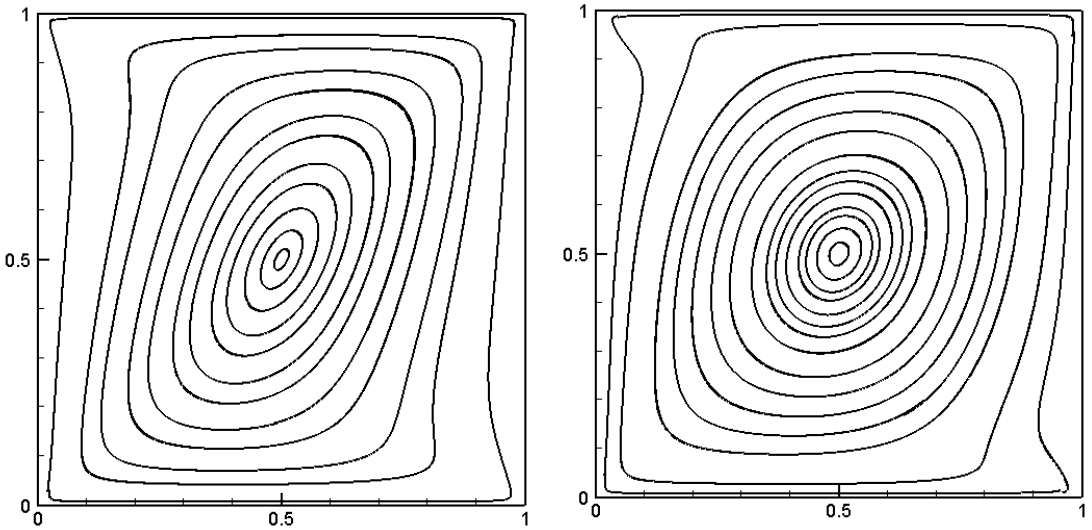

(a) *Re* = 100 (b) *Re* = 400

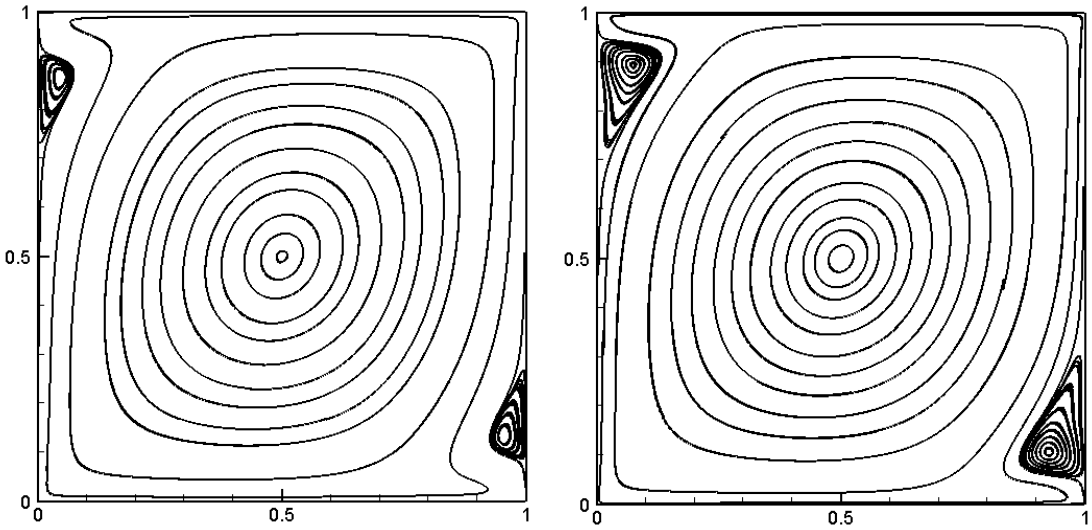

(c) *Re* = 1000 (d) *Re* = 2000

Figure 10. Streamline pattern for antiparallel wall motion at (a) *Re* = 100 (b) *Re* = 400 (c) *Re* = 1000 and (d) *Re* = 2000 on a 257 × 257 grid.

It has also been observed that the primary vortex centre remains very close to the geometric centre of the cavity even for these higher values of *Re* = 1000 and 2000. However the size of the secondary vortices are seen to increase between *Re* = 1000 and 2000. Similar increase in the size of the secondary vortices with Reynolds numbers was also observed for the parallel wall motion. Figure 11 shows the vorticity contours for various Reynolds numbers. A magnified view of the secondary vortices (the ones at the top left corner) at *Re* = 1000 is shown in Figure 12. Figures 13-16 show the plots of horizontal velocity profiles along vertical lines and vertical velocity profiles along horizontal lines passing through different points of the square cavity for the various Reynolds numbers. Table 2 gives the locations of the vortex centres for *Re* = 100, 400, 1000, 1500 and 2000. For the same reasons mentioned in the previous sub-section, these results should be sufficiently accurate.

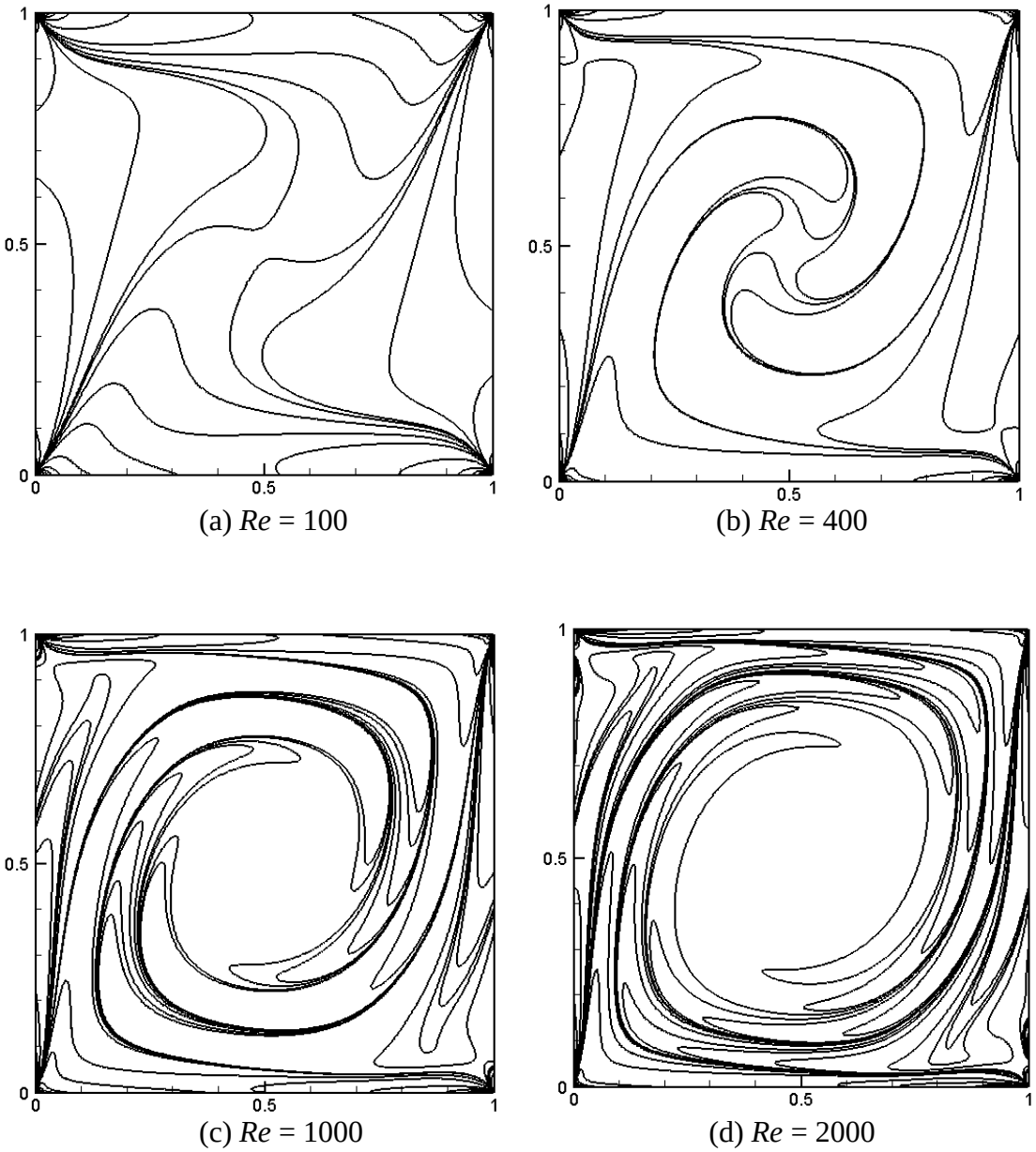

(a) *Re* = 100 (b) *Re* = 400

(c) *Re* = 1000 (d) *Re* = 2000

Figure 11. Vorticity contours for antiparallel wall motion at (a) *Re* = 100 (b) *Re* = 400 (c) *Re* = 1000 and (d) *Re* = 2000 on a 257 × 257 grid.

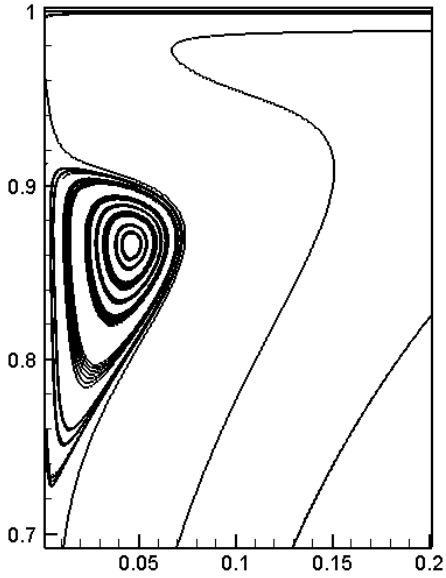

Figure 12. A magnified view of the secondary vortex at the top-left corner for antiparallel wall motion (*Re* = 1000).

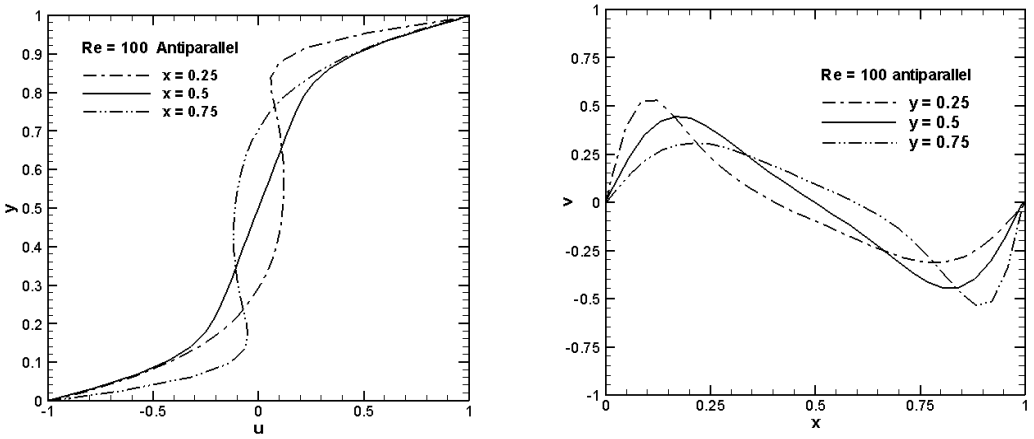

Figure 13. Antiparallel wall motion, *Re* = 100: (a) horizontal velocity *u* along vertical lines (*x*=0.25, 0.50 and 0.75), (b) vertical velocity *v* along horizontal lines (*y*=0.25, 0.50 and 0.75).

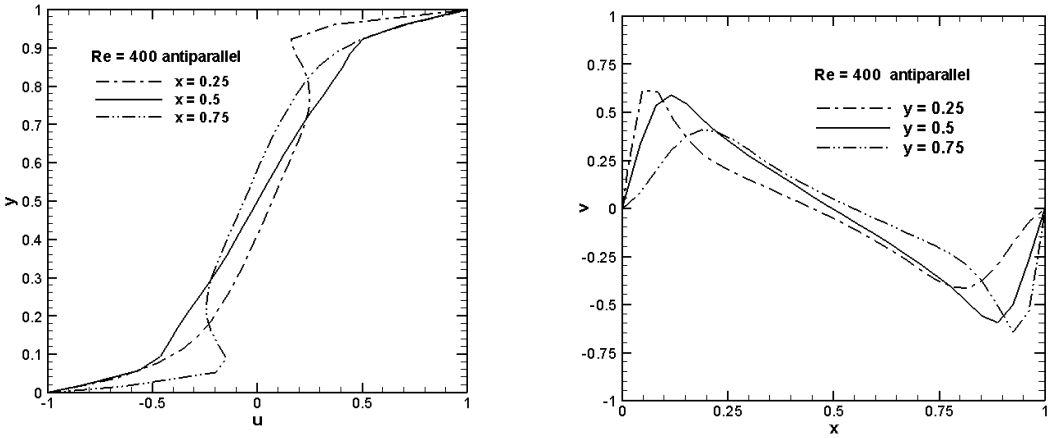

Figure 14. Antiparallel wall motion, *Re* = 400: (a) horizontal velocity *u* along vertical lines (*x*=0.25, 0.50 and 0.75), (b) vertical velocity *v* along horizontal lines (*y*=0.25, 0.50 and 0.75).

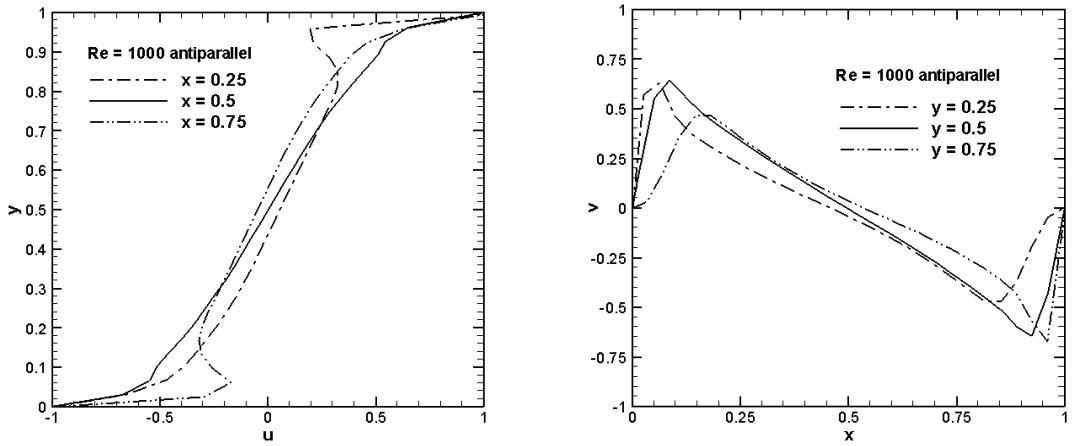

Figure 15. Antiparallel wall motion, *Re* = 1000: (a) horizontal velocity *u* along vertical lines (*x*=0.25, 0.50 and 0.75), (b) vertical velocity *v* along horizontal lines (*y*=0.25, 0.50 and 0.75).

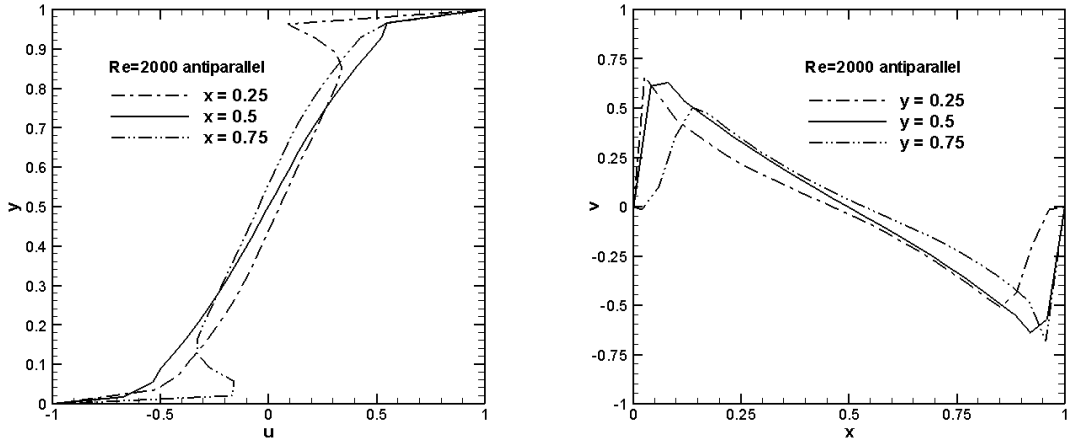

Figure 16. Antiparallel wall motion, *Re* = 2000: (a) horizontal velocity *u* along vertical lines (*x*=0.25, 0.50 and 0.75), (b) vertical velocity *v* along horizontal lines (*y*=0.25, 0.50 and 0.75).

TABLE 2: LOCATIONS OF THE VORTICES FOR ANTIPARALLEL WALL MOTION USING FDM.

Re	Primary Vortex (PV)		Secondary Vortices (SV)			
			Bottom Right		Top Left	
	x	*y*	*x*	*y*	*x*	*y*
100	0.5001	0.5002	…	…	…	…
400	0.5002	0.4981	…	…	…	…
1000	0.5009	0.4980	0.9507	0.1319	0.0492	0.8663
1500	0.5007	0.4982	0.9308	0.1156	0.0692	0.8856
2000	0.5002	0.5001	0.9227	0.1082	0.0771	0.8920

4. Conclusion

In this work the flow in an unexplored configuration, the two-sided lid-driven square cavity for the parallel and anti-parallel wall motion is computed with the FDM. This flow configuration is fraught with many interesting issues in that in the case of parallel wall motion it involves development of a pair of off-corner vortices and a free shear layer and in the case of anti-parallel wall motion it exhibits corner vortices that appear at a lower Reynolds number compared with the single-sided lid-driven cavity. The FDM code for the stream function-vorticity form of the Navier-Stokes equations based on central differencing and ADI time integration is developed. This code has second order spatio-temporal accuracy and it is used to produce steady results in a time-marching fashion. The FDM-based code is first validated through a careful comparison exercise with established results so that the results for the present configuration enjoy credibility. The results include figures and tables that record the details of several flow features like position of the vortex centres and their sizes. As the present computations for the flow situations explored have no predecessor, these results provide an important basis to investigators to compare their results with.

References

[1] Shankar, P.N, and M.D. Deshpande, Fluid Mechanics in the Driven Cavity. Annual Review of Fluid Mechanics, 2000. **32**: p. 93-136.

[2] Bruneau, C.H., and M. Saad, The 2D lid-driven cavity problem revisited. Computers & Fluids, 2006. **35**: p. 326-348.

[3] Gupta, M.M., and J.C. Kalita, A new paradigm for solving Navier-Stokes equations: Streamfunction-Velocity formulation. Journal of Computational Physics, 2005. **207**: p. 52-68.

[4] Burggraf, O.R., Analytical and numerical studies of the structure of steady separated flows. Journal of Fluid Mechanics, 1966. **24**: p. 113-151.

[5] Pan, F., and A. Acrivos, Steady flows in rectangular cavities. Journal of Fluid Mechanics, 1967. **28**: p. 643-655.

[6] Cheng, M., and K.C. Hung, Vortex structure of steady flow in a rectangular cavity. Computers & Fluids, 2006. **35**: p. 1046-1062.

[7] Ghia U., K.N. Ghia, and C.T. Shin, High-Re solutions for incompressible flow using Navier-Stokes equations and a multigrid method. Journal of Computational Physics, 1982. **43**: p. 387-411.

[8] Kuhlmann H.C., M. Wanschura, and H.J. Rath, Flow in two-sided lid-driven cavities: non-uniqueness, instability, and cellular structures. Journal of Computational Physics, 1997. **336**: p. 267-299.

[9] Blohm C.H., and H.C. Kuhlmann, The two-sided lid-driven cavity: experiments on stationary and time-dependent flows. Journal of Fluid Mechanics, 2002. **450**: p. 67-95.

[10] Albensoeder S., H.C. Kuhlmann, and H.C, Rath, Multiplicity of Steady Two-Dimensional Flows in Two-sided Lid-Driven Cavities. Theoretical Computational Fluid Dynamics, 2001. **14**: p. 223-241.

[11] Kalita J.C., A.K. Dass and D.C. Dalal, A transformation-free HOC scheme for steady convection-diffusion on Nonuniform grid. International Journal for Numerical Methods in Engineering, 2004. **38**: p. 3497-3521.

[12] Kumar N., J.C. Kalita and A.K. Dass. HOC computation of Two-Sided Lid-Driven Cavity Flow. in 2006 Proceedings of the Int. Conference on Computational Mechanics and Simulation, ICCMS 2006. 2006. IIT Guwahati, INDIA.

[13] Peaceman, D.W, and H.H. Rathford, The Numerical solution of parabolic and elliptic differential equations. Journal of the Society for Industrial and Applied Mathematics, 1955. **3**: p. 28-41.